Chemical Science

EDGE ARTICLE

View Article Online
View Journal | View Issue

Cite this: *Chem. Sci.*, 2019, **10**, 6278

All publication charges for this article have been paid for by the Royal Society of Chemistry

Construction and interconversion of anion-coordination-based ('aniono') grids and double helicates modulated by counter-cations†

Xiaoxia Fan,‡[a] Dan Zhang,‡[a] Shiyu Jiang,[a] Heng Wang,[b] Lin-Ting Lin,[c] Bo Zheng,[a] Wen-Hua Xu,[a] Yanxia Zhao,[a] Benjamin P. Hay,[d] Yi-Tsu Chan,[c] Xiao-Juan Yang,*[a] Xiaopeng Li[b] and Biao Wu*[a]

Received 23rd April 2019
Accepted 15th May 2019

DOI: 10.1039/c9sc02012h

rsc.li/chemical-science

Supramolecular assembly of well-defined discrete architectures has been of great interest due to the tunable properties of these structures in functional materials and bio-mimicking. While metal-coordination-driven assembly has been extensively studied, anion-coordination-driven assembly (ACDA) is just emerging for constructing complex supramolecular structures. Herein two $A_{2n}L_{2n}$ (A = anion, L = ligand; n = 1 or 2) 'aniono'-supramolecular assemblies, *i.e.* double helicates and the first anion grid, have been constructed based on the coordination between phosphate (PO_4^{3-}) anion and a bis–tris(urea) ligand. Moreover, the aniono-grid and double helicate motifs can be readily interconverted under ambient conditions by simply changing the counter-cation. These results redefine the power and scope of ACDA, which may represent a new approach in the assembly of well-defined architectures in parallel with the metal coordination-driven assembly of metallo-supramolecules.

Introduction

Assembly of supramolecular architectures plays an active role in the fields of functional materials and bio-mimicking.[1] A broad array of discrete structures has been constructed based on metal-coordination-driven assembly, such as helicates, polygons, polyhedra, cages, and interlocked metallo-supramolecules.[2] Meanwhile, such architectures can be accessed by (dynamic) covalent bonding[3] or hydrogen bonding.[4] During the assembling process, interconversion between two topologies in some systems, *e.g.*, double helicates and mononuclear complexes,[5] tetrahedral cages and triple helicates,[6] and many others,[7] has also been studied in terms of the dynamic functions of different structures.[8] Among the various entities, helical and grid complexes are highly interesting due to their specific topologies and properties.[9] As mimics of the helical motifs in DNA and proteins, synthetic helicates have fascinated supramolecular chemists with applications in molecular recognition, catalysis, molecular machines, optics, *etc.*[10] With specific arrangement of metal ions within a square or rectangular grid, metallo-grids have been explored in magnetic and electrochemical materials as well as in supramolecular host–guest chemistry.[11]

Compared to the flourishing metal-coordination-driven assembly, anion-coordination-driven assembly (ACDA) is less developed, yet it provides an efficient approach to construct well-defined structures.[12] In particular, the coordination between phosphate ions (PO_4^{3-}) and oligourea ligands has proven to be surprisingly stable.[13] As such, we were able to construct a series of anion-based architectures with phosphate ions as the coordination centers and oligo-bis(urea) as the ligands, such as the first A_2L_3 triple helicate and both face-directed A_4L_4- and edge-directed A_4L_6-type (A denotes anion) tetrahedral cages.[14] More recently, we further demonstrated the interconversion between the A_2L_3 triple helicate and A_4L_6 cage.[15] These results imply that the 'aniono'-supramolecular assemblies might become a new class of superstructures in parallel with the 'metallo'-systems. In addition, held together by multiple hydrogen bonds, these metal-free 'aniono'-systems are more bio-compatible, and their assembly–disassembly and isomerization may be readily modulated under mild conditions. However, compared to the well-established metal coordination, there are far fewer known anion complexes that exhibit the stability, predictable geometry, and symmetry needed to form such assemblies.[16] These features render ACDA very attractive but also highly challenging.

In the pursuit of more complex anion-based systems, we move forward from the bis–bis(urea)[17] to the bis–tris(urea) unit.[18] The

[a]*Key Laboratory of Synthetic and Natural Functional Molecule Chemistry of the Ministry of Education, College of Chemistry and Materials Science, Northwest University, Xi'an 710127, China. E-mail: yangxiaojuan@nwu.edu.cn; wubiao@nwu.edu.cn*

[b]*Department of Chemistry, University of South Florida, Tampa, FL 33620, USA*

[c]*Department of Chemistry, National Taiwan University, Taipei 10617, Taiwan*

[d]*Supramolecular Design Institute, Oak Ridge, TN 37830, USA*

† Electronic supplementary information (ESI) available: Synthetic procedures, characterization data and corresponding CIF files. CCDC 1892629–1892631. For ESI and crystallographic data in CIF or other electronic format see DOI: 10.1039/c9sc02012h

‡ These authors contributed equally to this work.

tris(urea) subunit exhibits stronger coordination affinity than the bis(urea) and forms stable AL_2 phosphate complexes with binding constants even comparable to those of some metal complexes.[18a] In addition, the coordination geometry of these complexes is analogous to the 2 : 1 metal complexes of terpyridine (tpy) (Scheme 1a), a versatile subunit for metal-based supramolecular assembly.[19] This analogy suggests that the 1 : 2 phosphate–tris(urea) complex is a potentially viable motif for anion-directed assembly with more predictable structures. Moreover, symmetry-constrained, *de novo* structure-based design methods[20] suggested that the *p*-xylylene-linked bis–tris(urea) **L** exhibited a conformation that complemented an A_2L_2 helical assembly (Fig. S1†). In this work, ligand **L** readily forms the double helicate and first anion-directed grid complex. Herein we report the crystal structures and solution assembly of these assemblies (Scheme 1b). The double helicate motif features a large, partially open cavity that is ideal for guest encapsulation and exchange, much like the grooves of DNA. Moreover, the grid and double helicate are easily interconverted by changing the counter-cation. Note that the switch between the M_2L_2 double helicates and 2 × 2 (M_4L_4) grid complexes had not been reported until recently when Lehn *et al.* described the first example of such an interconversion between a binuclear Cu^I double helicate and a tetranuclear Cu^{II} grid.[21] Hence, the current work also represents the first 'anion version' of the double helicate/grid interconversion and broadens the spectrum of ACDA in supramolecular transformation.

Results and discussion

Synthesis, structures, and solution studies of the double helicate 1a and grid complex 2

Complex 1a. Treatment of ligand **L** with 1 equiv. of $(TMA)_3PO_4$ (TMA^+ = tetramethylammonium) in acetonitrile, followed by slow vapor diffusion of diethyl ether, afforded yellow block crystals of $(TMA)_5[(TMA)\subset(PO_4)_2L_2]$ (**1a**). As expected, a two-stranded structure is obtained. However, instead of the predicted C_i symmetric double mesocate geometry (Fig. S1b†), complex **1a** exhibits less symmetric helical A_2L_2 assemblies, which might originate from the non-centrosymmetric tetrahedral TMA^+ guest (Fig. 1). The two PO_4^{3-} centers within one helix adopt the same configuration (ΛΛ shown in Fig. 1), but the complex is racemic (space group $P2_1/c$) with half of the supramolecules showing the opposite configurations. Although complex **1a** lacks strict symmetry, the two ligands show very similar conformations and a non-distorted geometry would have one C_2 axis perpendicular to the P···P axis, but no C_2 axis through the two PO_4^{3-} centers. Each phosphate ion is coordinated by six urea groups (herein from two tris-urea units) through twelve hydrogen bonds (Fig. 1b and Table S2†). The two ligand strands are considerably twisted to form a large, partially open 'cage' in the middle of the helix, in which a TMA^+ cation is encapsulated with N···P distances to the two phosphate ions of 5.10 and 5.38 Å, respectively (Scheme 1b). This 'helicate cage' is indeed similar to that formed in the A_2L_3 triple helicate with the methylene biphenylene-spaced bis–bis(urea) ligand,[17b] in which the ligands are also folded and compressed to accommodate a TMA^+ guest (with N···P distances of 6.26 and 6.42 Å). The TMA^+ ion is bound by electrostatic force and cation–π interactions with two phenyl rings of the *p*-xylylene spacer (purple-dashed lines, N···centroid distances are 4.426 Å to R1 and 4.340 Å to R2; Fig. 1c). The remaining five TMA^+ ions serve as counter cations and are located around the helix (Fig. S12†).

In the assembly of anion-centered double helicates, the first one was constructed with polyguanidinium ligands and sulfate

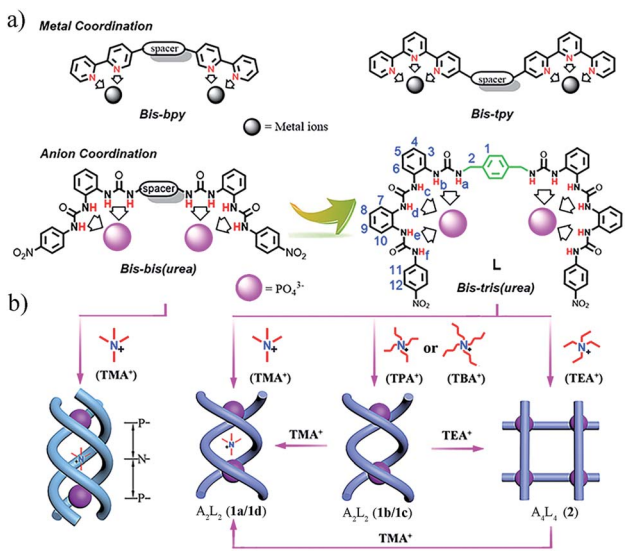

Scheme 1 (a) Design of bis–bis(urea) and bis–tris(urea) ligands by mimicking oligopyridine–metal coordination; (b) triple helicate assembled by bis–bis(urea) ligands and $TMA_3(PO_4)$;[14a] A_2L_2 double helicate (complexes **1a–1d**) and A_4L_4 grid (complex **2**) (A = anion, L = ligand) assembled by the bis–tris(urea) ligand **L** and PO_4^{3-} in the presence of different tetraalkylammonium cations.

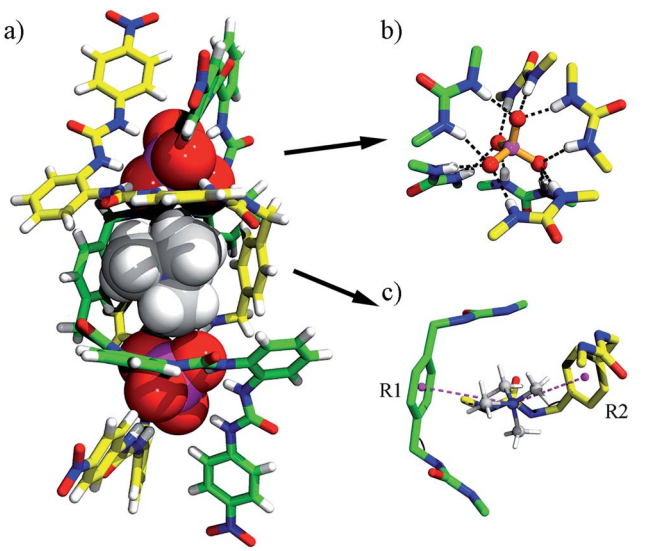

Fig. 1 (a) Crystal structure of the double helicate $[(TMA)\subset(PO_4)_2L_2]^{5-}$ (**1a**); (b) hydrogen bonds between a PO_4^{3-} ion and six urea units; (c) a TMA^+ ion is encapsulated in the central cavity through cation–π interactions (purple-dashed lines; R1 and R2 denote the centroids of the aryl rings that are involved in cation–π interactions). Only an M enantiomer is shown; other counter cations and solvents are omitted for clarity.

ions in solution.[22] Later, several other double helicates based on halide anions were reported, *e.g.*, the fluoride-directed helicate with neutral amide ligands[23] and chloride-directed double helix with pyrrole-based oligomers.[24] Very recently, Flood *et al.* reported the interconversion of single (foldamers) and double helicates glued by anions.[25] However, complex **1a** is the first double helicate with PO_4^{3-} anions.

The assembly of **L** and PO_4^{3-} ions and the encapsulation of TMA^+ in solution was investigated by 1D and 2D NMR and ESI-MS. Compared to the free ligand, all the urea NH groups in complex **1a** show significant downfield shifts ($\Delta\delta$ = 2.89–3.91 ppm, NMR of ligand **L** was measured in DMSO-d_6 for solubility reasons; Fig. 2b), corresponding to the coordination of urea to phosphate. A characteristic upfield shift of the H12 proton on the terminal nitrophenyl group ($\Delta\delta = -0.54$ ppm; proton numbering, see Scheme 1a) is observed because of the strong shielding effects imposed in the helical structure. Interestingly, the two protons from one methylene of the spacer (H2) appear at different resonances due to their non-equivalent environments owing to the lack of symmetry in the double helicate (Fig. 1). This was also proved by 2D COSY which reveals the correlation between the two split peaks, indicating that they are from the same carbon (Fig. S25†).

Notably, in the room-temperature NMR spectrum, there is only one peak for the two types of cations, *i.e.*, encapsulated and peripheral TMA^+ ions. This peak appears at an 'averaged' position of 2.80 ppm, only slightly upfield-shifted ($\Delta\delta = -0.28$ ppm) relative to free TMA^+ (3.08 ppm) in $(TMA)_3PO_4$, possibly due to the fast exchange between peripheral and trapped TMA^+ guests at the NMR time scale. However, when the temperature is lowered to 233 K the peaks of ligands **L** split into two sets, indicating that the molecular motion is 'frozen' and the guest is 'fastened' (Fig. 2c). Meanwhile, the two different types of TMA^+ cations become distinguishable, with the 'missing' signal of the trapped TMA^+ (H_α) now showing a much more upfield shift at δ 1.64 ppm ($\Delta\delta = -1.44$ ppm compared to the free state; see Fig. S9–S11† for variable-temperature ^{1}H NMR). In contrast, the protons of the five peripheral TMA^+ ions (2.97 ppm) only shifted slightly upfield ($\Delta\delta = -0.11$ ppm), revealing the lack of shielding on these ions, with an appropriate ratio (5 : 1) of the integral for the two types of TMA^+ ions.

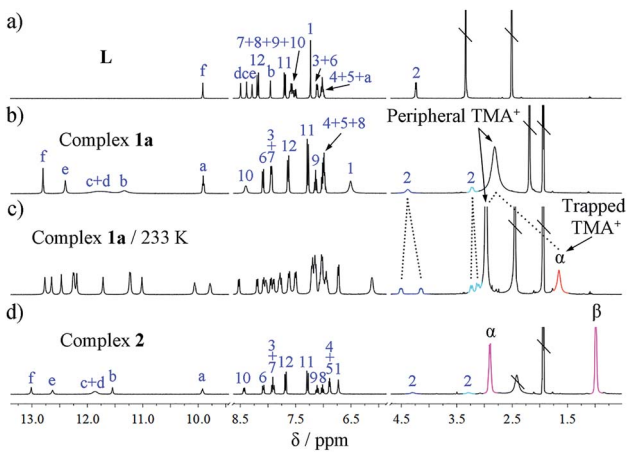

Fig. 2 ^{1}H NMR spectra (400 MHz) of (a) ligand **L** in DMSO-d_6, 296 K; (b) double helicate **1a** in CD_3CN, 296 K; (c) **1a** in CD_3CN, 233 K; and (d) grid **2** in CD_3CN, 296 K. Signals of the two hydrogens of the methylene linker are shown in blue and turquoise, while that of trapped TMA^+ ion is shown in red and protons of TEA^+ in deep pink, respectively; \ represents solvent residue.

2D NMR spectra provide further evidence for the TMA^+ cation encapsulation by the clear ^{1}H–^{1}H NOE (nuclear Overhauser effect) correlations between H_α of TMA^+ and the phenylene protons (H1) of the linker of **L** (see Scheme 1 for proton numbering; Fig. S26†). The formation of a single host–guest species was confirmed by DOSY (diffusion-ordered nuclear magnetic resonance spectroscopy) (Fig. S27†). The HR ESI-MS spectrum of complex **1a** also supports the formation of the A_2L_2 complex. Specifically, intense peaks at m/z 804.6570 ($x = 3$) and 1244.0363 ($x = 4$) corresponding to various $A_2L_2(TMA)_n$ species, such as $[(PO_4)_2L_2(TMA)_x]^{(6-x)-}$, are seen in the spectrum (Fig. 4a).

Complex 2. By treating ligand **L** with 1.0 equiv. of $(TEA)_3PO_4$ that contains the larger TEA^+ (tetraethylammonium) cation, the first anion-coordination-based grid complex, $(TEA)_{10}[(TEA)_2\subset(PO_4)_4L_4]$ (**2**), was obtained. Its X-ray structure clearly shows a tetranuclear square conformation with four PO_4^{3-} ions positioned at the corners and four ligand molecules spanning the edges, two of which (opposite, magenta and bright green) are above the anion centers and the other two (yellow and cyan) are below (Fig. 3a). As required by a typical grid, the two diagonal PO_4^{3-} centers show the same chirality that is contrary to the other two corners, and the whole molecule (centrosymmetric space group $I4_1/a$) is achiral with alternating configurations ($\Delta\Lambda\Delta\Lambda$). The coordination sphere of PO_4^{3-} ions consists of six urea groups from two tris(urea) subunits that donate twelve hydrogen bonds to phosphate (Fig. 3c and Table S4†). Although known metal-directed M_4L_4 assemblies usually exhibit D_4 symmetries,[20b] this anion-directed A_4L_4 analogue exhibits S_4 symmetry, and the four symmetry-related PO_4^{3-} ions deviate slightly from co-planarity (by 0.58 Å), constituting a tilted square with four identical P···P distances of 11.95 Å and P···P···P angles of 89.5°.

The negative charges of the anionic grid are balanced by twelve TEA^+ counter-cations, which reside in four different environments. Notably, inside the grid, two TEA^+ cations (type I) are readily accommodated, with one sitting over the other, an arrangement adopted possibly to facilitate cation···π interactions with the 'aromatic box' around them (Fig. 3b and S18a†). The two type-II TEA^+ ions (distributed to four half-occupancy positions) are located at each vertex of the grid, forming hydrogen bonds with the terminal nitro groups (Fig. 3a and S18b†). Notably, each ligand strand as the 'edge' of grid **2** is folded to a helical conformation spanning *ca.* 1.5 turns. Within each ligand helix, a 'half cavity' is formed to encapsulate one of the third-type TEA^+ cations (type III), which is surrounded by four aryl rings of the 'host' ligand and complemented by a terminal nitrophenyl plane from a neighboring ligand (Fig. S18a†). Finally, the remaining four TEA^+ ions (type-IV) each cap a phosphate corner of the grid, forming intra- and intermolecular interactions with ligand aromatic rings, thus

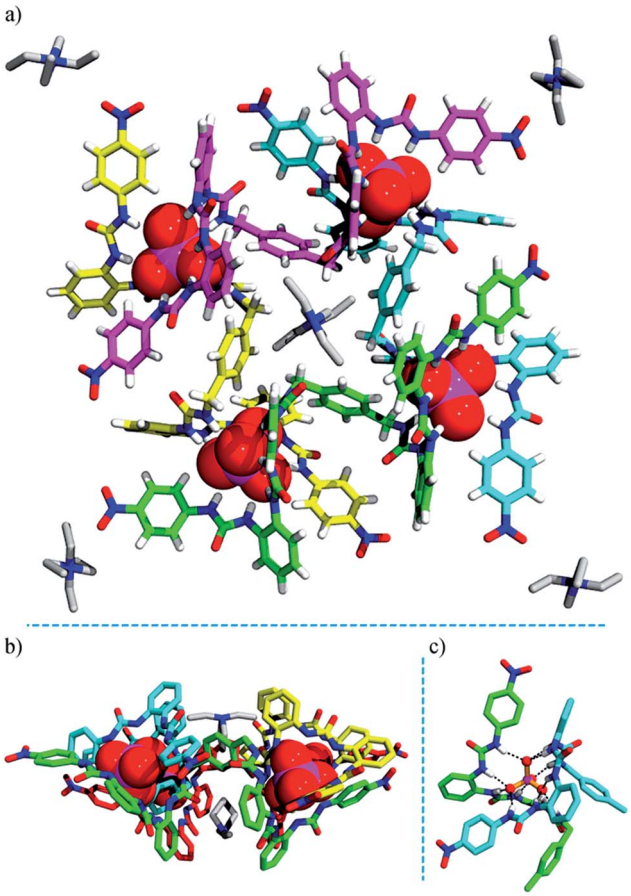

Fig. 3 Crystal structure of the heterochiral (ΔΛΔΛ) grid complex **2** $(TEA)_{10}[(TEA)_2\subset(PO_4)_4L_4]$. (a) Top view; (b) side view; (c) hydrogen bonds formed between a PO_4^{3-} ion and six urea units. Some TEA^+ cations are omitted for clarity (see Fig. S18† for the locations and interactions of these counter ions).

linking two grids (Fig. S19†). All these cations, either internal or 'peripheral', may provide important templating or additional stabilizing effects for the grid structure, which also imply the possible guest inclusion ability of the voids in the grid complex **2**.

In the ^{1}H NMR spectrum of grid **2**, the urea NH groups also show large downfield shifts ($\Delta\delta = 2.93$–4.14 ppm; Fig. 2d). The signal of the aryl H12 proton ($\Delta\delta = -0.49$ ppm) undergoes an obvious upfield shift. The two protons from one CH_2 group of the spacer also split into two doublets due to their different chemical environments. Notably, although the crystal structure of **2** shows four different locations of TEA^+ cations, they appear as only one set of signals in the NMR spectrum. Both of the CH_2 (H_α) and CH_3 (H_β) signals of TEA^+ shift slightly upfield compared to that of the free $(TEA)_3PO_4$ ($\Delta\delta_\alpha = -0.28$ ppm and $\Delta\delta_\beta = -0.20$ ppm) (Fig. 2d), and there is no significant change when the temperature is lowered (down to 233 K). This might reflect the facts that (a) there is a fast exchange among the protons at the four locations; and (b) these cations indeed form similar interactions with ligand **L** as revealed by the crystal structure. On the other hand, the HR ESI-MS spectrum confirms the composition of the A_4L_4 complex with the stoichiometry $[(TEA)_9(PO_4)_4L_4]^{3-}$ (obsd 1851.9443 and cald 1851.8676, Fig. 4b). It is evident that complexes **1a** and **2** display different NMR and ESI-MS signals, which can be used to distinguish the configuration of the double helicate or grid (see also the red dotted box in Fig. 5a).

Assembly of the double helicates 1b and 1c

Considering the different outcomes in the two cases where only the counter cation varies, it appears that the counter cation (as the guest) plays a critical role in determining the supramolecular assembling process. To further elucidate the effect of the cation, we studied the assembly of **L** with one equivalent of $(TPA)_3PO_4$ or $(TBA)_3PO_4$ which contains the larger tetraalkylammonium homologues (TPA = tetrapropylammonium; TBA = tetrabutylammonium). In both cases, crystalline products (complexes **1b** and **1c**) were yielded. Although single crystals suitable for X-ray diffraction could not be obtained despite many attempts, the configuration of these complexes can be identified by a combination of ^{1}H NMR, HR ESI-MS, and theoretical calculations. The two products show ^{1}H NMR features that are similar to each other (Fig. 5a) but different from those of either complex **1a** or **2**, and the methylene H2 protons of the linker do not show any split, implying no significant guest interaction with the host. Their ESI-MS spectra are also similar, revealing a 2 : 2 anion-to-ligand ratio (Fig. S21 and S22†). Thus,

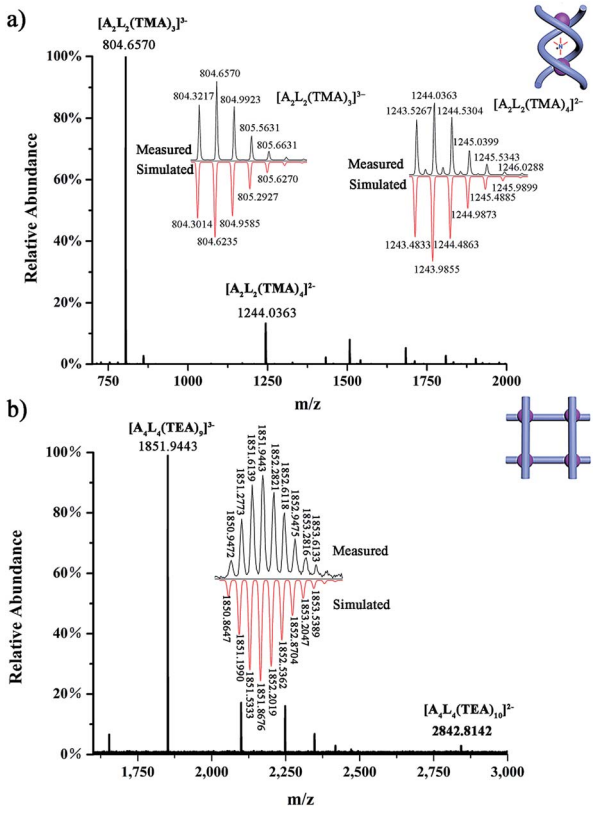

Fig. 4 HR ESI-MS spectra of (a) complex $(TMA)_5[(TMA)\subset(PO_4)_2L_2]$ (**1a**); and (b) complex $(TEA)_{10}[(TEA)_2\subset(PO_4)_4L_4]$ (**2**).

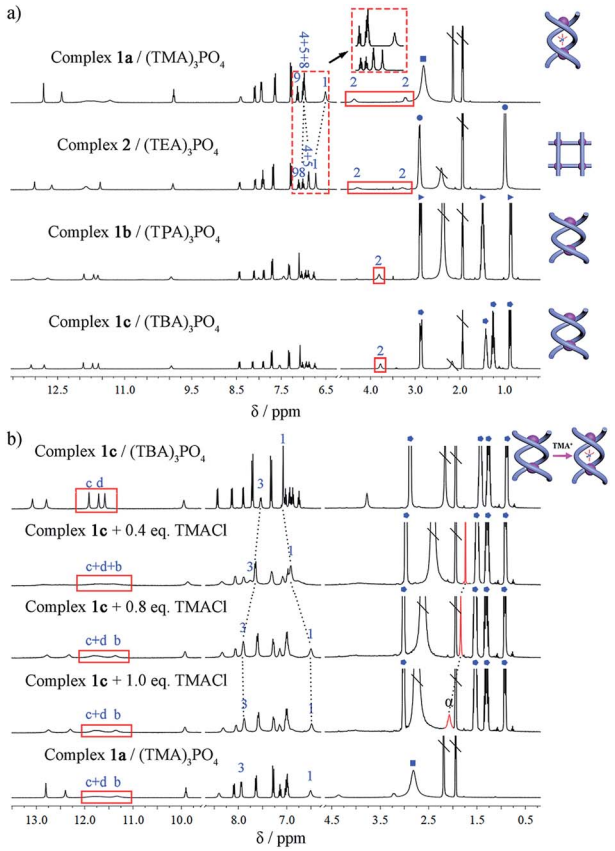

Fig. 5 ^{1}H NMR spectra demonstrating the assembly of different phosphate salts with ligand **L** (400 MHz, CD_3CN, 296 K). (a) **L** with 1 equiv. of $(TMA)_3PO_4$, $(TEA)_3PO_4$, $(TPA)_3PO_4$ or $(TBA)_3PO_4$. (b) Stacking spectra of complexes **1a** and **1c**, and titration of **1c** with (TMA)Cl (■ denotes signals for TMA^+, ● for TEA^+, ▶ for TPA^+, and ⬢ for TBA^+. The signal of trapped TMA^+ is shown in red; \ represents solvent residue).

we speculate that both complexes may have the double-stranded configuration, either double helicate or mesocate, with an 'empty' central cavity (solvent-filled) because either TPA or TBA is too large to fit. DFT calculations yield representative geometries for the helicate (Fig. S28†) and mesocate (Fig. S29†) assemblies in the absence of a guest. In the former case, optimization of the observed helicate geometry suggests that although the cavity becomes slightly smaller, the double helicate structure persists after the guest is removed.

Interconversion between the double helicate and grid motifs

Indeed, the guest-free complexes **1b/c** provide an ideal model to examine the templating effect of the cation. For complex **1c**, $[(TBA)_6(PO_4)_2\mathbf{L}_2]$, when (TMA)Cl was titrated in, the NMR spectrum gradually changed to that of the double helicate **1a**. The methylene protons split into two peaks, and the encapsulation of TMA^+ ions can be monitored. With the addition of less than 1 equiv. of TMA^+ ions (per A_2L_2 unit) to complex **1c**, the methyl signal H_α showed a dramatic upfield resonance at 1.74 ppm ($\Delta\delta = -1.34$ ppm compared to free TMA^+), indicating the encapsulation of TMA^+. However, this signal shifted back downfield when more than 1 equiv. of TMA^+ cations was added (Fig. 5b), which was caused by the fast exchange of the encapsulated and excess peripheral TMA^+ cations, as in the case of complex **1a**. Finally, with more TMA^+ cations (6 equiv.), the titration reached saturation and the spectrum is almost the same as that of **1a**.

Inspired by the NMR titration results, which indicated that the initially 'empty' double helicate $(TBA)_6[(PO_4)_2\mathbf{L}_2]$ (**1c**) can encapsulate one TMA^+ cation (and thus displace one TBA^+ ion), we were able to isolate single crystals of the double helicate complex **1d**, $(TBA)_5[(TMA)\subset(PO_4)_2\mathbf{L}_2]$ (Fig. S16 and Table S3†) from **L** and a mixture of phosphate salts of TMA^+ and TBA^+ in a 1 : 5 ratio. The main structure $[(TMA)\subset(PO_4)_2\mathbf{L}_2]^{5-}$ in **1d** is essentially the same as that in complex **1a**, and the difference lies only in the peripheral counter cations, TBA^+ in **1d** *versus* TMA^+ in **1a**. In addition, HR ESI-MS also shows the signal of $[(TBA)_3(TMA)(PO_4)_2\mathbf{L}_2]^{2-}$ (*m/z* obsd 1496.3825 *versus* calcd 1496.2675, Fig. S20†).

Subsequently, the conversion of double helicate to grid motifs was studied using ^{1}H NMR titration (Fig. 6a) by introducing the TEA^+ ions into helicate **1c**. With the addition of 1 equiv. of (TEA)Cl to a solution of **1c** in CD_3CN, the methylene protons H2 of the spacer split to two peaks, a characteristic feature of grid **2**. In the aromatic area, the H1 signal shifts upfield due to encapsulation of a TEA^+ ion with the conformational change. Meanwhile, both peaks of TEA^+ appear in the

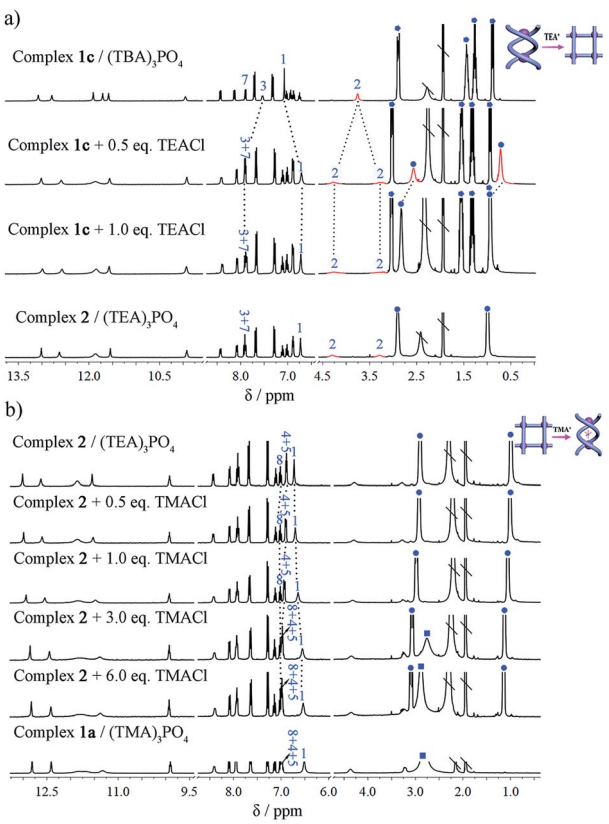

Fig. 6 Partial ^{1}H NMR titration spectra demonstrating the interconversion of different complexes (400 MHz, CD_3CN, 296 K). (a) From 'empty' double helicate to grid **2** by titrating **1c** with (TEA)Cl. (b) From grid **2** to double helicate **1a** by titrating complex **2** with (TMA)Cl (■ denotes signals for TMA^+, ● for TEA^+, and ⬢ for TBA^+. Signals of trapped TEA^+ ions are shown in red; \ represents solvent residue).

upfield region (without peripheral TEA^+ ions) compared to those of complex **2** but shift downfield gradually with more added TEA^+ ions until becoming identical to complex **2**. On the other hand, the reverse process, *i.e.* transformation of the grid structure **2** to double helicate (**1a**) is also readily realized upon addition of the TMA^+ template (Fig. 6b). With the encapsulation of TMA^+, the aryl H1 signal of the spacer shifts slightly upfield until reaching the same as complex **1a**, and H4 and H5 peaks shift downfield due to the deshielding effect after encapsulation of the TMA^+.

Thus, we have observed the conversion not only from complexes **1b**/**c** to **1a**, namely from 'empty' to the TMA^+-filled double helicate, but also from **1b**/**c** to grid **2** under the modulation of TEA^+ cations. Conversely, due to the strong binding of the helical cage to TMA^+, transformation of grid **2** to double helicate **1a** is also very feasible. Such template-induced supramolecular transformations have also been reported for metal-coordination driven assembly, in which the counter-anions are responsible for the conformational changes.[2c,6c,7d,9a,b]

Conclusions

We reported the design and synthesis of a C_2-symmetric bis–tris(urea) ligand with a *p*-xylylene linker, which is assembled with a phosphate anion to form the first anion coordination-based 2×2 grid (A_4L_4) and a double helicate (A_2L_2) featuring an open cavity similar to DNA grooves. Moreover, facile interconversion between these two motifs can be realized simply by modulation with the counter-cation under ambient conditions, which is also complementary to anion-controlled structural interconversion. This work reveals the power of anion coordination in supramolecular assembly. Such anion-o-supramolecular systems could be a new class of architectures for promising applications in many fields. Construction of more complex structures and exploration of their functionality is currently underway.

Conflicts of interest

The authors declare no competing financial interest.

Acknowledgements

This work was supported by the National Natural Science Foundation of China (21772154, 91856102 and 21771144). BPH acknowledges the sponsorship from the 100 Talents Award, Shaan'xi Province.

Notes and references

1 (*a*) B. H. Northrop, Y.-R. Zheng, K.-W. Chi and P. J. Stang, *Acc. Chem. Res.*, 2009, **42**, 1554–1563; (*b*) M. D. Pluth and K. N. Raymond, *Chem. Soc. Rev.*, 2007, **36**, 161–171; (*c*) W. Xuan, C. Zhu, Y. Liu and Y. Cui, *Chem. Soc. Rev.*, 2012, **41**, 1677–1695; (*d*) M. Han, D. M. Engelhard and G. H. Clever, *Chem. Soc. Rev.*, 2014, **43**, 1848–1860; (*e*) E. Yashima, N. Ousaka, D. Taura, K. Shimomura, T. Ikai and K. Maeda, *Chem. Rev.*, 2016, **116**, 13752–13990; (*f*) T. Hasell and A. I. Cooper, *Nat. Rev. Mater.*, 2016, **1**, 16053; (*g*) S. Datta, M. L. Saha and P. J. Stang, *Acc. Chem. Res.*, 2018, **51**, 2047–2063.

2 (*a*) M. Fujita, M. Tominaga, A. Hori and B. Therrien, *Acc. Chem. Res.*, 2005, **38**, 369–378; (*b*) R. W. Saalfrank, H. Maid and A. Scheurer, *Angew. Chem., Int. Ed.*, 2008, **47**, 8794–8824; (*c*) I. A. Riddell, M. M. J. Smulders, J. K. Clegg, Y. R. Hristova, B. Breiner, J. D. Thoburn and J. R. Nitschke, *Nat. Chem.*, 2012, **4**, 751–756; (*d*) M. M. J. Smulders, I. A. Riddell, C. Browne and J. R. Nitschke, *Chem. Soc. Rev.*, 2013, **42**, 1728–1754; (*e*) T. R. Cook and P. J. Stang, *Chem. Rev.*, 2015, **115**, 7001–7045; (*f*) X. Jing, C. He, L. Zhao and C. Duan, *Acc. Chem. Res.*, 2019, **52**, 100–109; (*g*) Y. Lu, H.-N. Zhang and G.-X. Jin, *Acc. Chem. Res.*, 2018, **51**, 2148–2158.

3 (*a*) H. Li, H. Zhang, A. D. Lammer, M. Wang, X. Li, V. M. Lynch and J. L. Sessler, *Nat. Chem.*, 2015, **7**, 1003; (*b*) X. Wang, Y. Wang, H. Yang, H. Fang, R. Chen, Y. Sun, N. Zheng, K. Tan, X. Lu, Z. Tian and X. Cao, *Nat. Commun.*, 2016, **7**, 12469; (*c*) H. Qu, Y. Wang, Z. Li, X. Wang, H. Fang, Z. Tian and X. Cao, *J. Am. Chem. Soc.*, 2017, **139**, 18142–18145.

4 (*a*) G. Portella, M. W. Germann, N. V. Hud and M. Orozco, *J. Am. Chem. Soc.*, 2014, **136**, 3075–3086; (*b*) L. B. Favero, W. Li, L. Spada, L. Evangelisti, G. Visentin and W. Caminati, *Chem.–Eur. J.*, 2015, **21**, 15970–15973.

5 (*a*) Y. Yao, M. W. Perkovic, D. P. Rillema and C. Woods, *Inorg. Chem.*, 1992, **31**, 3956–3962; (*b*) V. Amendola, L. Fabbrizzi, L. Gianelli, C. Maggi, C. Mangano, P. Pallavicini and M. Zema, *Inorg. Chem.*, 2001, **40**, 3579–3587.

6 (*a*) W. Meng, T. K. Ronson, J. K. Clegg and J. R. Nitschke, *Angew. Chem., Int. Ed.*, 2013, **52**, 1017–1021; (*b*) X.-Z. Li, L.-P. Zhou, L.-L. Yan, D.-Q. Yuan, C.-S. Lin and Q.-F. Sun, *J. Am. Chem. Soc.*, 2017, **139**, 8237–8244; (*c*) T. Zhang, L.-P. Zhou, X.-Q. Guo, L.-X. Cai and Q.-F. Sun, *Nat. Commun.*, 2017, **8**, 15898.

7 (*a*) S. Chen, L.-J. Chen, H.-B. Yang, H. Tian and W. Zhu, *J. Am. Chem. Soc.*, 2012, **134**, 13596–13599; (*b*) A. J. McConnell, C. S. Wood, P. P. Neelakandan and J. R. Nitschke, *Chem. Rev.*, 2015, **115**, 7729–7793; (*c*) W. Wang, Y.-X. Wang and H.-B. Yang, *Chem. Soc. Rev.*, 2016, **45**, 2656–2693; (*d*) H. B. T. Jeazet, K. Gloe, T. Doert, O. N. Kataeva, A. Jager, G. Geipel, G. Bernhard, B. Buchner and K. Gloe, *Chem. Commun.*, 2010, **46**, 2373–2375.

8 (*a*) H. Miyake and H. Tsukube, *Chem. Soc. Rev.*, 2012, **41**, 6977–6991; (*b*) S. Otto, *Acc. Chem. Res.*, 2012, **45**, 2200–2210; (*c*) M. Barboiu, A.-M. Stadler and J.-M. Lehn, *Angew. Chem., Int. Ed.*, 2016, **55**, 4130–4154.

9 (*a*) B. Hasenknopf, J.-M. Lehn, B. O. Kneisel, G. Baum and D. Fenske, *Angew. Chem., Int. Ed.*, 1996, **35**, 1838–1840; (*b*) B. Hasenknopf, J.-M. Lehn, N. Boumediene, A. Dupont-Gervais, A. Van Dorsselaer, B. Kneisel and D. Fenske, *J. Am. Chem. Soc.*, 1997, **119**, 10956–10962; (*c*) M. Fujita, *Chem. Soc. Rev.*, 1998, **27**, 417–425; (*d*) S. Leininger, B. Olenyuk and P. J. Stang, *Chem. Rev.*, 2000, **100**, 853–908; (*e*) H. Juwarker and K.-S. Jeong, *Chem. Soc. Rev.*, 2010, **39**,

3664–3674; (*f*) J. G. Hardy, *Chem. Soc. Rev.*, 2013, **42**, 7881–7899.

10 (*a*) J.-m. Suk, V. R. Naidu, X. Liu, M. S. Lah and K.-S. Jeong, *J. Am. Chem. Soc.*, 2011, **133**, 13938–13941; (*b*) Y. Hua, Y. Liu, C.-H. Chen and A. H. Flood, *J. Am. Chem. Soc.*, 2013, **135**, 14401–14412; (*c*) Y. Ferrand and I. Huc, *Acc. Chem. Res.*, 2018, **51**, 970–977; (*d*) M. Albrecht and S. Kotila, *Angew. Chem., Int. Ed.*, 1996, **35**, 1208–1210; (*e*) M. Albrecht, *Chem.–Eur. J.*, 2000, **6**, 3485–3489; (*f*) J. Sahoo, R. Arunachalam, P. S. Subramanian, E. Suresh, A. Valkonen, K. Rissanen and M. Albrecht, *Angew. Chem., Int. Ed.*, 2016, **55**, 9625–9629.

11 (*a*) M. Albrecht, *Chem. Rev.*, 2001, **101**, 3457–3498; (*b*) M. Ruben, J. Rojo, F. J. Romero-Salguero, L. H. Uppadine and J.-M. Lehn, *Angew. Chem., Int. Ed.*, 2004, **43**, 3644–3662; (*c*) S. Dhers, A. Mondal, D. Aguilà, J. Ramírez, S. Vela, P. Dechambenoit, M. Rouzières, J. R. Nitschke, R. Clérac and J.-M. Lehn, *J. Am. Chem. Soc.*, 2018, **140**, 8218–8227.

12 (*a*) K. Bowman-James, *Acc. Chem. Res.*, 2005, **38**, 671–678; (*b*) K. M. Mullen and P. D. Beer, *Chem. Soc. Rev.*, 2009, **38**, 1701–1713; (*c*) R. Custelcean, *Chem. Soc. Rev.*, 2014, **43**, 1813–1824; (*d*) P. A. Gale, E. N. W. Howe and X. Wu, *Chem*, 2016, **1**, 351–422; (*e*) Y. Liu, C. Hu, A. Comotti and M. D. Ward, *Science*, 2011, **333**, 436–440; (*f*) A. E. Hargrove, S. Nieto, T. Zhang, J. L. Sessler and E. V. Anslyn, *Chem. Rev.*, 2011, **111**, 6603–6782; (*g*) Q. He, P. Tu and J. L. Sessler, *Chem*, 2018, **4**, 46–93.

13 (*a*) B. P. Hay, T. K. Firman and B. A. Moyer, *J. Am. Chem. Soc.*, 2005, **127**, 1810–1819; (*b*) D. Yang, J. Zhao, X.-J. Yang and B. Wu, *Org. Chem. Front.*, 2018, **5**, 662–690; (*c*) J. Zhao, D. Yang, X.-J. Yang and B. Wu, *Coord. Chem. Rev.*, 2019, **378**, 415–444.

14 (*a*) S. Li, C. Jia, B. Wu, Q. Luo, X. Huang, Z. Yang, Q.-S. Li and X.-J. Yang, *Angew. Chem., Int. Ed.*, 2011, **50**, 5721–5724; (*b*) B. Wu, F. Cui, Y. Lei, S. Li, N. d. S. Amadeu, C. Janiak, Y.-J. Lin, L.-H. Weng, Y.-Y. Wang and X.-J. Yang, *Angew. Chem., Int. Ed.*, 2013, **52**, 5096–5100; (*c*) W. Zuo, Z. Huang, Y. Zhao, W. Xu, Z. Liu, X.-J. Yang, C. Jia and B. Wu, *Chem. Commun.*, 2018, **54**, 7378–7381.

15 X. Bai, C. Jia, Y. Zhao, D. Yang, S.-C. Wang, A. Li, Y.-T. Chan, Y.-Y. Wang, X.-J. Yang and B. Wu, *Angew. Chem., Int. Ed.*, 2018, **57**, 1851–1855.

16 C. J. Massena, D. A. Decato and O. B. Berryman, *Angew. Chem., Int. Ed.*, 2018, **57**, 16109–16113.

17 (*a*) B. Wu, S. Li, Y. Lei, H. Hu, N. d. S. Amadeu, C. Janiak, J. S. Mathieson, D.-L. Long, L. Cronin and X.-J. Yang, *Chem.–Eur. J.*, 2015, **21**, 2588–2593; (*b*) C. Jia, W. Zuo, D. Yang, Y. Chen, L. Cao, R. Custelcean, J. Hostaš, P. Hobza, R. Glaser, Y.-Y. Wang, X.-J. Yang and B. Wu, *Nat. Commun.*, 2017, **8**, 938.

18 (*a*) C. Jia, B. Wu, S. Li, Z. Yang, Q. Zhao, J. Liang, Q.-S. Li and X.-J. Yang, *Chem. Commun.*, 2010, **46**, 5376–5378; (*b*) S. Li, M. Wei, X. Huang, X.-J. Yang and B. Wu, *Chem. Commun.*, 2012, **48**, 3097–3099.

19 (*a*) J.-P. Sauvage, J.-P. Collin, J.-C. Chambron, S. Guillerez, C. Coudret, V. Balzani, F. Barigelletti, L. De Cola and L. Flamigni, *Chem. Rev.*, 1994, **94**, 993–1019; (*b*) U. S. Schubert and C. Eschbaumer, *Angew. Chem., Int. Ed.*, 2002, **41**, 2892–2926.

20 (*a*) B. P. Hay, *Chem. Soc. Rev.*, 2010, **39**, 3700–3708; (*b*) N. J. Young and B. P. Hay, *Chem. Commun.*, 2013, **49**, 1354–1379.

21 A.-M. Stadler, C. Burg, J. Ramírez and J.-M. Lehn, *Chem. Commun.*, 2013, **49**, 5733–5735.

22 J. Sánchez-Quesada, C. Seel, P. Prados, J. de Mendoza, I. Dalcol and E. Giralt, *J. Am. Chem. Soc.*, 1996, **118**, 277–278.

23 S. J. Coles, J. G. Frey, P. A. Gale, M. B. Hursthouse, M. E. Light, K. Navakhun and G. L. Thomas, *Chem. Commun.*, 2003, 568–569.

24 Y. Haketa and H. Maeda, *Chem.–Eur. J.*, 2011, **17**, 1485–1492.

25 Y. Liu, F. C. Parks, W. Zhao and A. H. Flood, *J. Am. Chem. Soc.*, 2018, **140**, 15477–15486.